NANO LETTERS

Letter

pubs.acs.org/NanoLett

Materials Processing Routes to Trap-Free Halide Perovskites

Andrei Buin, Patrick Pietsch, Jixian Xu, Oleksandr Voznyy, Alexander H. Ip, Riccardo Comin, and Edward H. Sargent*

Department of Electrical and Computer Engineering, The University of Toronto, Toronto, ON M5S 3G4, Canada

Supporting Information

ABSTRACT: Photovoltaic devices based on lead iodide perovskite films have seen rapid advancements, recently achieving an impressive 17.9% certified solar power conversion efficiency. Reports have consistently emphasized that the specific choice of growth conditions and chemical precursors is central to achieving superior performance from these materials; yet the roles and mechanisms underlying the selection of materials processing route is poorly understood. Here we show that films grown under iodine-rich conditions are prone to a high density of deep electronic traps (recombination centers), while the use of a chloride precursor avoids the formation of key defects (Pb atom substituted by I) responsible for short diffusion lengths and poor photovoltaic performance. Furthermore, the lowest-energy surfaces of perovskite crystals are found to be entirely trap-free, preserving both electron and hole delocalization to a remarkable degree, helping to account for explaining the success of polycrystalline perovskite films. We construct perovskite films from I-poor conditions using a lead acetate precursor, and our measurement of a long (600 ± 40 nm) diffusion length confirms this new picture of the importance of growth conditions.

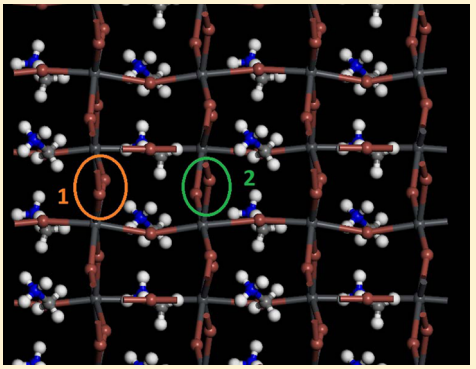

KEYWORDS: *Perovskite, defect, electronic traps, diffusion length, growth, precursor*

Solar cells based on a methylammonium lead triiodide ($MA-PbI_3$, $MA{=}CH_3NH_3$) organic/inorganic perovskite active layer have attracted considerable interest in view of their potential as low-cost, high-efficiency photovoltaic (PV) materials.[1−4] One of the most remarkable features of these materials is their exceptionally long carrier diffusion length (L_D), which in the very best cases can be as high as 1 μm.[5] This enables a rare and valuable quality in a solution-processed semiconductor: a transport length that exceeds the absorption length for photon energies exceeding the semiconductor's bandedge, leading to wavelengths of light above the semiconductor's bandedge, leading to reduced recombination losses and improved photocurrents. The large values of L_D allow for the fabrication of high-efficiency devices by removing the need for bulk heterojunctions, enabling planar active layers architectures[2] which minimize surface recombination and increase open-circuit voltage. However, it has been reported that it is principally only those $MA-PbI_3$ films that are fabricated from a mixture of lead-chloride ($PbCl_2$) and methylammonium-iodide (MA−I) precursors that exhibit the most such impressive transport properties for the photogenerated carriers,[2] whereas single-halide approaches yield L_D ∼ 100 nm. The origin of this behavior, which is unrelated to the final film composition (found to be the same for mixed- and single-halide growth[2,6−8]), is key to understanding and controlling these promising materials, but has not yet been identified.

In an effort to resolve this enigma, we use density functional theory (DFT) to explore the electronic levels and formation energies of trap and defect states as the perovskite $MA-PbI_3$ film is grown from its precursors. This methodology provides a powerful framework for studying the impact of composition on the bandstructure of crystals incorporating vacancies, dopants, and interfaces. It is particularly important to identify and classify those localized, in-gap states which may capture the photogenerated carriers and deteriorate the power conversion efficiency of PV materials. We classify shallow traps as those lying between 0 and 10 kT inside the gap from the nearest bandedge, where T is the material's temperature and k is Boltzmann's constant, and deep traps as $E_{trap} > 10\ kT$. While the former mainly affects the carrier mobility, the latter strongly captures both electrons and holes, producing accelerated recombination which is highly detrimental to PV performance. While previous DFT studies of organometallic halides have been reported,[3,6,7,9−20] here we elucidate the trap formation mechanisms and energetics in Pb-based perovskites under a range of various experimental growth conditions. Ultimately, we find a striking correlation between the choice of precursors and the density of trap states in the final compound, revealing that how an I-poor growth environment is key for high PV performance.

We performed DFT calculations on tetragonal $MA-PbI_3$ by using a supercell including 1728 atoms, which can accom-

Received: July 10, 2014
Revised: September 21, 2014

   dx.doi.org/10.1021/nl502612m | *Nano Lett.* XXXX, XXX, XXX−XXX

modate various types of lattice and substitutional sparse defects. In line with previous reports,[6,17,21] the electronic structure is confirmed to be direct at the Γ-point, with a valence band maximum (VBM) state in an antibonding combination of I 5p (dominant character) and Pb 6p orbitals (Pb 6s−I 5p, σ^*), while the conduction band minimum (CBM) has mainly Pb 6p character (see Methods and SI for more details).

The first part of our study aims at exploring the impact of the nanocrystalline morphology on the bandstructure of MA−PbI_3. In particular, one of the remarkable features of these materials is that, in spite of their polycrystallinity, they have exceedingly sharp bandedges.[22] We carried out electronic structure calculations on slabs of perovskite crystals to evaluate the impact of surfaces on their bandstructure. The corresponding density of states (Figure 1a) shows no states in the gap either for bulk or surface electronic structure. Indeed the highest-lying valence band states in asymmetrically terminated stoichiometric slabs (Figure 1b) exhibit a high degree of delocalization, as do the lowest-lying conduction band states (Figure 1c). A crucial insight into the origin of this behavior comes from the computed surface energies: very low values of ∼10 meV/Å^2 are obtained (SI). The low surface energy indicates high stability, obviating the need for a reconstruction of the (001) terminated surface and also avoiding the need to add adsorbates (e.g., introduce new ligands) in order to remain inert. It was shown recently[23] that the surface energy of terminated (001) PbI_2 slabs is indeed small and compares quite well to our value of surface energy (see also SI).

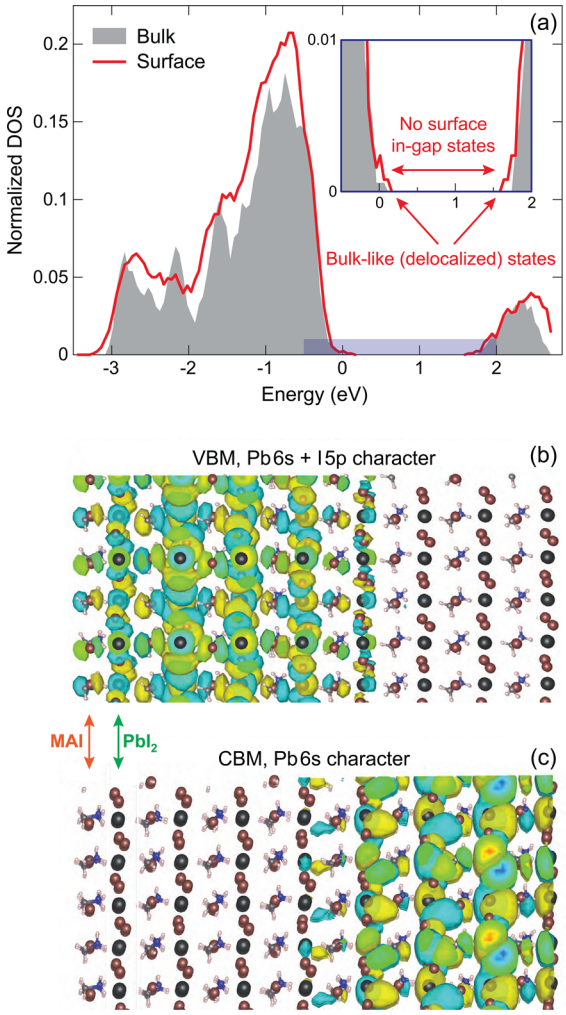

Figure 1. Surface states of the Pb halide perovskites. (a) The density of states for an 16-monolayer slab (surface) compared to the case of bulk materials. The inset reveals that no electronic states emerge in the slab compared to the bulk. The wave functions of surface states at (b) the valence band maximum (VBM) remain highly delocalized in the case of 16-monolayer slabs, similarly to those at (c) the conduction band minimum (CBM) states. The highest amplitudes of positive- (negative-) valued wave functions are indicated in yellow (blue). Please note that the CBM and VBM states are separated due to asymmetric termination.

For the second part, we turn our attention to defects. This required first to estimate the formation energy of the perovskite relative to its decomposition into pure PbI_2 and MAI phases (Figure 2a). Our calculations show that the formation energy of the perovskite relative to its decomposition into pure PbI_2 and MAI phases has a low value of about −0.1 eV. This indicates that the material and its precursors are close to phase coexistence of MAI and PbI_2 which is consistent with recent experimental findings[24,25] of a residual PbI_2 phase even after long annealing times. It is also consistent with reports[19,24,26−30] that the details of preparation conditions are important to achieve the best-performing materials.

We then proceeded to analyze the electronic levels (Figure 2b) and formation energies (H_f) of various classes of defects, such as vacancies (V_{Pb}, V_{MA}, V_I), interstitials (Pb_i, MA_i, I_i), and antisites (Pb_I, I_{Pb}), where in the latter case A_B indicates that A is substituted by B (the required corrections for the various charged states are discussed in the SI). The value of H_f allows us to estimate the density of the relevant vacancy species, which will be proportional to $\exp(-H_f/kT)$. One can see from Figure 3a and b (see also Supplementary Table 4) that the major acceptor defects are V_{Pb}^{-2}, V_{MA}^{-1} and I_i^{-1}, while donor defects are V_I^{+1} and Pb_i^{+2}, with an associated charge density sufficient to induce doping anywhere from p- to n-type, depending on the chemical potentials. Defects V_I^{+1}, V_{MA}^{-1}, and MA_i^{+1} possess the lowest formation energies over the entire bandgap. The transition levels of V_{Pb}^{-1} and I_i^{-1} (see SI) are located on top of the VBM, indicating that negative charge states are stable over the entire bandgap. The defect formation energies of neutral defects are given in Supplementary Table 4. One can also see that Pb_i, Pb_I, and I_{Pb} represent the "negative-U" defects,[31,32] indicating that these defects are not stable at +1, −1, and +2 charge states, respectively. The large structural relaxation in the case of Pb_I^0 (interplanar I−I−I bridging) is consistent with such "negative-U" behavior of the charge neutral Pb_I antisite. Figure 3a and b also shows defect states with negative formation energies at various Fermi levels. Usually, this implies that at these chemical potentials and Fermi levels it is not possible to grow the crystal, and Fermi level pinning happens in a such way that all of the defect energies are positive[33] while satisfying the overall charge-neutrality condition; in other words, the structure is not stable for such parameters.[33−37] However, these are values of the single defect formation energies, and nothing prevents the complexation of single defects whenever the latter is favorable in energy. Thus, defect clustering expands the range of chemical potentials and Fermi levels, i.e., growth conditions. So far, the complex defect formation has been reported in case of V_{PbI_2} alone[38] and shown recently to have low formation energies.[39] We find that all vacancies produce either slightly perturbed states in the bands (which do not capture carriers), or shallow traps and resonances (deep localized states

dx.doi.org/10.1021/nl502612m | Nano Lett. XXXX, XXX, XXX−XXX

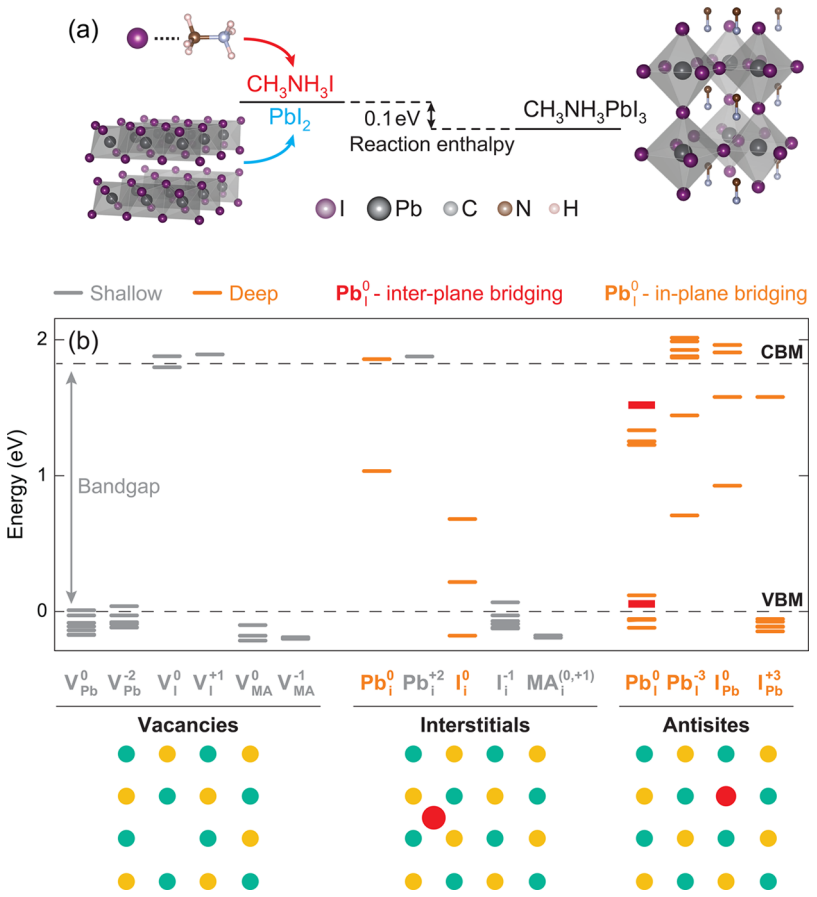

Figure 2. Tetragonal perovskite, its formation from experimentally employed precursors, and its defect energy levels. (a) The energy of formation of the $CH_3NH_3PbI_3$ perovskite (room temperature tetragonal structure is shown) from its bulk precursors CH_3NH_3I and PbI_2, with a kinetic barrier (transition state energy) also depicted. Calculations discussed in the text report a −0.1 eV difference between the perovskite and its precursors, consistent with experimental studies that show the presence of a secondary PbI_2 phase. (b) Energy levels associated with the defect states corresponding to neutral and charged vacancies (V_{Pb}, V_I, V_{MA}), neutral and charged interstitials (Pb_i, I_i, MA_i), and neutral and charged states associated with antisites (Pb_I and I_{Pb}).

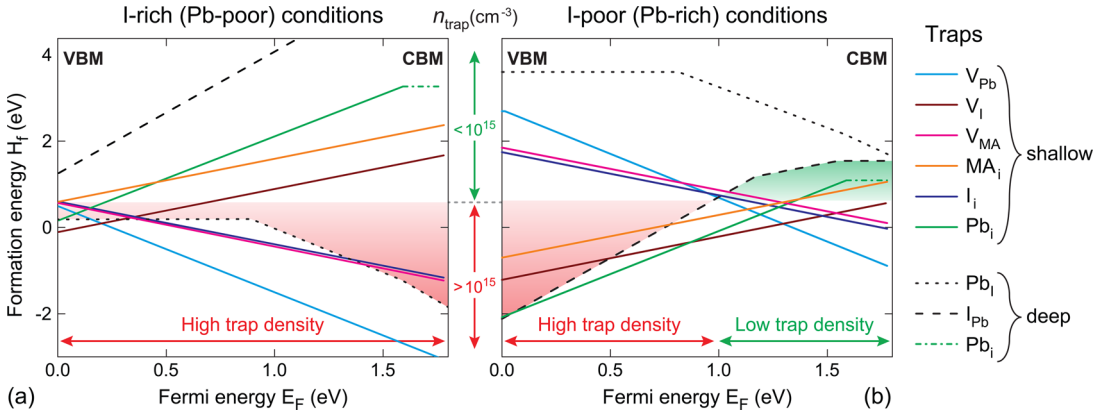

Figure 3. Formation energies and volume densities of key defects in tetragonal lead perovskites. Defect formation energies for iodine-poor (a) and iodine-rich (b) growth conditions. Continuous (dashed) lines denote shallow (deep) traps (see legend). The red region in (a) indicates the range of Fermi energies where trap densities exceed 10^{18} cm^{-3}—showing that no Fermi level choice yields a semiconductor substantially free of deep traps in the case of I-rich growth conditions. Conversely, in the case of I-poor growth (b), trap densities below 10^{15} cm^{-3} can be achieved in the range of Fermi energies (green region). In case of MA-related defects one has (a) MA-poor and (b) MA-rich conditions.

hybridized with conduction or valence band states[40]) within the band, implying that carriers can still relax easily to VBM and CBM. In contrast, certain interstitials and antisites associated with Pb and I form electronic states deep inside the bandgap. The most important figure of merit is the density of deep traps in the semiconductor volume, which will determine the rate of capture of charge carriers and of loss due to recombination. In semiconductors having good electronic transport parameters, it is indeed the density of recombination centers that directly controls the diffusion length of charge carriers.[41,42]

dx.doi.org/10.1021/nl502612m | Nano Lett. XXXX, XXX, XXX−XXX

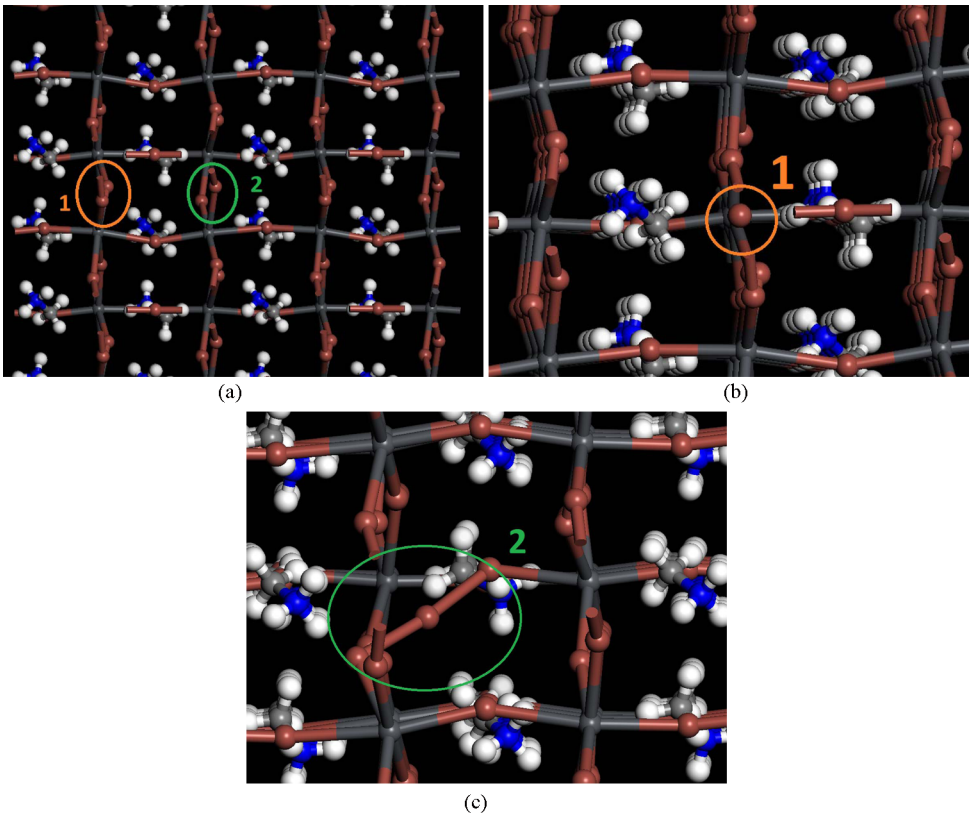

Figure 4. Physical configuration of Pb_I neutral antisites in the tetragonal phase. (a) Two different PbI_2 planes in the tetragonal phase. One of them is bulged. Upon structural relaxation of the Pb_I^0 defect, two conformations are possible: (b) in-plane bridging or (c) interplanar bridging. The bridge configuration has a motif very similar to the I_3^- triiodide complex, with an I−I−I angle of 172° and bond length 2.98 Å. This allows us to associate the Pb_I^0 neutral antisite with the presence in solution-phase precursors of the macro-ion complexes such as PbI_3^- and PbI_4^{2-}, the latter expected to be present in growth under iodide-rich conditions.

Further analysis of the tetragonal vs cubic crystal phase leads to a small number of qualitatively and quantitatively different conclusions with respect to defect state energies. Overall the agreement with previously published results[19] is good, except that it was previously found that the Pb_I neutral antisite defect has a high formation energy in the cubic case. We show herein that, in the tetragonal phase, the Pb_I neutral antisite defect possess a much lower formation energy. Physically, this difference arises because in the tetragonal phase two distinct PbI_2 layers are found (Figure 4): a nearly planar PbI_2 plane and also a bulged PbI_2 plane. The methylammonium cation has been shown experimentally to exhibit a small reorientational barrier[43] and to possess a small energetic difference between two perovskite structures with different methylammonium cation orientations, thus affecting the structure of the PbI_2 layers.[6]

The formation energy for charged defects, and consequently the volume density of the various classes of localized electronic states, is a function of the Fermi level in the semiconductor. The former is determined by whether the crystal is grown from iodine-poor or iodine-rich conditions, which constitutes the central link between the growth chemistry and the charge transport performance of these materials. We found that in a crystal grown under I-rich conditions (Figure 3a), the Pb_I antisite (Pb atom replaced by I) deep trap has a formation energy of less than 0.2 eV for all choices of Fermi level between the valence and conduction bandedges, i.e., for all non-degenerate doping conditions. We predict that the perovskite grown under I-rich conditions will show a high density of deep traps that will curtail the diffusion length. In contrast, in a crystal grown under I-poor conditions (Figure 3b), there exists a window of Fermi levels, $E_F \geq 0.9$ eV (measured relative to the VBM), where all deep traps have formation energies that exceed 0.38 eV. This places the equilibrium density of trap states below 10^{15} cm^{-3}. At this volume density, traps are spaced a median ∼200 lattice constants in all crystallographic directions, enabling diffusion lengths above 100 nm. Such low trap densities are also consistent with the impressive open-circuit voltages seen in the best reported lead iodide perovskite devices.[2,24]

From a chemical perspective, the presence in solution of simple ions (Pb^{2+} and I^-) combined with that of lead-iodide complex anions such as PbI_3^-,[44] PbI_4^{2-}, and PbI_5^{3-} produces a motif similar to the Pb_I^0 neutral antisite defect which corresponds to bridging between three iodine anions in-plane (Figure 4b) and interplane (Figure 4c) in the perovskite lattice. The motif is produced indirectly, by violating local stoichiometry. The I−I−I angle is 172°, and the I···I bond length between two iodines is 2.98 Å. Knowledge of this geometry allows us to look for signatures of this complex, as does the signature wave function pattern (I 5p−I 5p, σ^*). The concentration of PbI_3^- in solution is higher for PbI_2 + MAI than for $PbCl_2$ + MAI (SI). One interesting direction these results suggest is that alternative Pb non-iodine-containing precursors, such as $Pb(SCN)_2$, $Pb(CH_3CH_2)_4$, and Pb acetate, can provide another avenue to reaching I-poor conditions required for high-quality perovskites.

dx.doi.org/10.1021/nl502612m | *Nano Lett.* XXXX, XXX, XXX−XXX

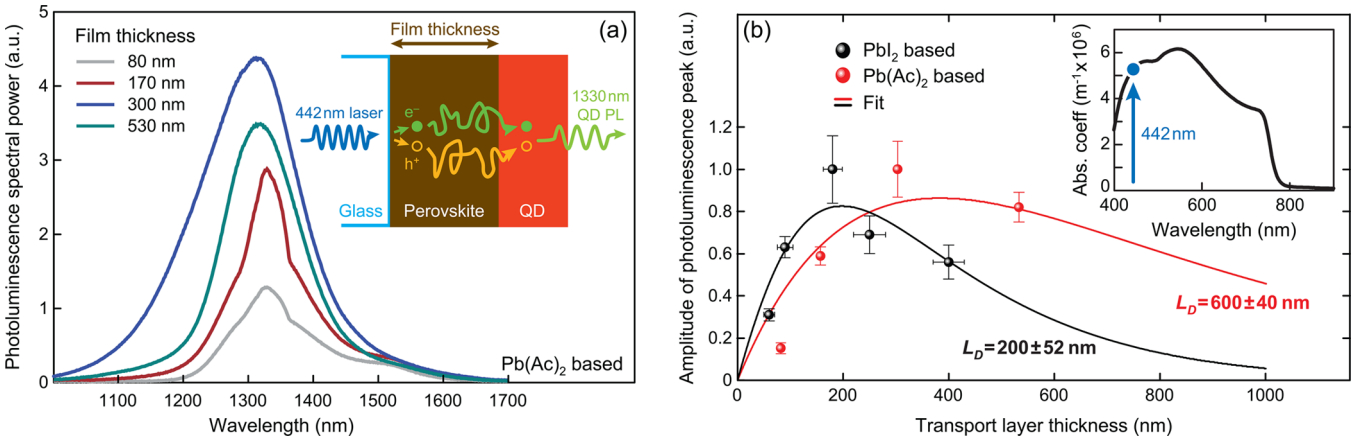

Figure 5. Experimental investigation of transport in novel iodide-poor perovskite films. (a) Measured photoluminescence (PL) spectra for various perovskite layer thicknesses as indicated in the legend in the case of $Pb(Ac)_2$ precursor. The inset shows a schematic of the diffusion length measurement method: the sample is illuminated at a wavelength (442 nm) that is strongly absorbed in the perovskite layer; photogenerated charge carriers diffuse to the quantum dot reporter layer where they recombine, providing a spectrally distinct signature of their arrival. (b) Experimental plot (black and red circles) of the corrected PL (see SI) peak amplitude vs perovskite layer thickness both for the PbI_2 and $Pb(Ac)_2$ precursors. A fit based on eq 1 allows estimating the diffusion length to be $L_D \approx 600$ nm and $L_D \approx 200$ nm, which is comparable to prior pure and mixed-halide films. Inset: measured absorption coefficient of the perovskite absorber, where the excitation wavelength is highlighted.

As a way to validate this prediction, and in order to challenge experimentally the proposed theoretical findings, we investigated the diffusion length in perovskite films formed using a lead acetate [$Pb(Ac)_2$] precursor in place of the typical PbI_2 or $PbCl_2$. The use of this precursor satisfies the requirement for I-poor conditions while providing a Cl-free platform in order to rule out any possible effect from residual amounts of incorporated chlorine. Similarly to the mixed-halide case, we find that acetate does not incorporate into the final product. In order to probe the diffusion lengths for MA–PbI_3 grown from $Pb(Ac)_2$, we excite our perovskite film using a 442 nm laser while measuring the photoluminescence (PL) signal in a reporter layer of small bandgap quantum dots (see inset of Figure 5a). The quantum dot PL intensity is directly controlled by the carrier diffusion length and by the thickness of the perovskite film[45] (see SI).

Qualitatively these diffusion length experiments can be understood as follows: for thin perovskite films with thickness d smaller than the carrier diffusion length L_D, the amplitude of the PL signal correlates positively with L_D, because an increase in layer thickness results in a higher absorption and hence a higher exciton generation rate, and at the same time almost all excitons can diffuse through the perovskite and reach the reporter layer. For increasing thickness, the generation rate reaches saturation because the absorption cannot exceed 100%, but fewer excitons can now diffuse to the reporter layer. The PL profiles for different perovskite film thicknesses are presented in Figure 5(a). The overall behavior of PL intensity vs film thickness (Figure 5b) can be modeled using the following function (see SI for derivation):

$$PL(d;\alpha,L_D) \propto \frac{L_D^2}{1-(\alpha L_D)^2}\left[\alpha e^{-\alpha d} + \frac{(e^{-\alpha d}/L_D)\sinh(d/L_D) - \alpha}{\cosh(d/L_D)}\right] \quad (1)$$

Here L_D is extracted by fitting the experimental data of Figure 5b once the independently measured absorption coefficient α is known (see inset). We determine the diffusion length of the $Pb(Ac)_2$ based perovskite films to be 600 nm, thus considerably larger than ~200 nm (even lower values of ~100 nm have been reported in literature[46]) for films formed using the PbI_2 precursor. This suggests that chlorine itself does not play a central role in large diffusion lengths, whereas the reduction of iodine content during the film formation process is likely key to the remarkable charge transport in these materials.

This study clarifies fundamental aspects underlying the impact of growth conditions on the performance of final MA–PbI_3 films. It reveals delocalization of the electronic states within the local nanocrystal surfaces that preserves the integrity of the bulk bandgap. The DFT-based analysis of defect formation energies provides an explanation for the observation of a larger charge diffusion length in perovskites prepared using iodide-free precursors[8,25,47–49] compared to MAI + PbI_2 growth conditions.

■ ASSOCIATED CONTENT

Supporting Information

Experimental methods. This material is available free of charge via the Internet at http://pubs.acs.org.

■ AUTHOR INFORMATION

Corresponding Author

*E-mail: ted.sargent@utoronto.ca.

Notes

The authors declare no competing financial interest.

■ ACKNOWLEDGMENTS

This publication is based in part on work supported by Award KUS-11-009-21, made by King Abdullah University of Science and Technology (KAUST), by the Ontario Research Fund Research Excellence Program, and by the Natural Sciences and Engineering Research Council (NSERC) of Canada. Computations were performed on the Southern Ontario Smart Computing Innovation Platform (SOSCIP) Blue Gene/Q supercomputer located at the University of Toronto's SciNet[50] HPC facility. The SOSCIP multiuniversity/industry consortium is funded by the Ontario Government and the Federal SciNet is

funded by the Canada Foundation for Innovation under the auspices of Compute Canada; the Government of Ontario; Ontario Research Fund—Research Excellence; and the University of Toronto. We thank Dr. Pongsakorn Kanjanaboos for AFM images and Dr. Zhijun Ning and Dr. Mingjian Yuan for the fruitful discussions.

REFERENCES

(1) Conings, B.; Baeten, L.; De Dobbelaere, C.; D'Haen, J.; Manca, J.; Boyen, H.-G. *Adv. Mater.* **2013**, *26*, 1−6.
(2) Liu, M.; Johnston, M. B.; Snaith, H. J. *Nature* **2013**, *501*, 395−398.
(3) Baikie, T.; Fang, Y.; Kadro, J. M.; Schreyer, M.; Wei, F.; Mhaisalkar, S. G.; Graetzel, M.; White, T. J. *J. Mater. Chem. A* **2013**, *1*, 5628−5641.
(4) Green, M. A.; Ho-Baillie, A.; Snaith, H. J. *Nat. Photonics* **2014**, *8*, 506−514.
(5) Stranks, S. D.; Eperon, G. E.; Grancini, G.; Menelaou, C.; Alcocer, M. J. P.; Leijtens, T.; Herz, L. M.; Petrozza, A.; Snaith, H. J. *Science* **2013**, *342*, 341−344.
(6) Mosconi, E.; Amat, A.; Nazeeruddin, M. K.; Gratzel, M.; De Angelis, F. *J. Phys. Chem. C* **2013**, *117*, 13902−13913.
(7) Colella, S.; Mosconi, E.; Fedeli, P.; Listorti, A.; Gazza, F.; Orlandi, F.; Ferro, P.; Besagni, T.; Rizzo, A.; Calestani, G.; Gigli, G.; De Angelis, F.; Mosca, R. *Chem. Mater.* **2013**, *25*, 4613−4618.
(8) You, J.; Hong, Z.; Yang, Y. M.; Chen, Q.; Cai, M.; Song, T.-B.; Chen, C.-C.; Lu, S.; Liu, Y.; Zhou, H.; Yang, Y. *ACS Nano* **2014**, *8*, 1674−1680.
(9) Umebayashi, T.; Asai, K.; Kondo, T.; Nakao, A. *Phys. Rev. B* **2003**, *67*, 155405.
(10) Borriello, I.; Cantele, G.; Ninno, D. *Phys. Rev. B* **2008**, *77*, 235214.
(11) Takahashi, Y.; Obara, R.; Lin, Z.-Z.; Takahashi, Y.; Naito, T.; Inabe, T.; Ishibashi, S.; Terakura, K. *Dalton Trans.* **2011**, *40*, 5563−5568.
(12) Chiarella, F.; Zappettini, A.; Licci, F.; Borriello, I.; Cantele, G.; Ninno, D.; Cassinese, A.; Vaglio, R. *Phys. Rev. B* **2008**, *77*, 045129.
(13) Chang, Y. H.; Park, C. H. *J. Korean Phys. Soc.* **2004**, *44*, 889−893.
(14) Brivio, F.; Walker, A. B.; Walsh, A. *APL Mater.* **2013**, *1*, 042111.
(15) Even, J.; Pedesseau, L.; Jancu, J.-M.; Katan, C. *J. Phys. Chem. Lett.* **2013**, *4*, 2999−3005.
(16) Quarti, C.; Grancini, G.; Mosconi, E.; Bruno, P.; Ball, J. M.; Lee, M. M.; Snaith, H. J.; Petrozza, A.; Angelis, F. D. *J. Phys. Chem. Lett.* **2014**, *5*, 279−284.
(17) Wang, Y.; Gould, T.; Dobson, J. F.; Zhang, H.; Yang, H.; Yao, X.; Zhao, H. *Phys. Chem. Chem. Phys.* **2014**, *16*, 1424−1429.
(18) Giorgi, G.; Fujisawa, J.-I.; Segawa, H.; Yamashita, K. *J. Phys. Chem. Lett.* **2013**, *4*, 4213−4216.
(19) Yin, W.-J.; Shi, T.; Yan, Y. *Appl. Phys. Lett.* **2014**, *10*, 063903.
(20) Kim, J.; Lee, S.-H.; Lee, J. H.; Hong, K.-H. *J. Phys. Chem. Lett.* **2014**, *5*, 1312−1317.
(21) Lindblad, R.; Bi, D.; Park, B.-w.; Oscarsson, J.; Gorgoi, M.; Siegbahn, H.; Odelius, M.; Johansson, E. M. J.; Rensmo, H. *J. Phys. Chem. Lett.* **2014**, *5*, 648−653.
(22) De Wolf, S.; Holovsky, J.; Moon, S.-J.; Lper, P.; Niesen, B.; Ledinsky, M.; Haug, F.-J.; Yum, J.-H.; Ballif, C. *J. Phys. Chem. Lett.* **2014**, *5*, 1035−1039.
(23) Haruyama, J.; Sodeyama, K.; Han, L.; Tateyama, Y. *J. Phys. Chem. Lett.* **2014**, *5*, 2903−2909.
(24) Burschka, J.; Pellet, N.; Moon, S.-J.; Humphry-Baker, R.; Gao, P.; Nazeeruddin, M. K.; Grätzel, M. *Nature* **2013**, *499*, 316−319.
(25) Liu, M.; Johnston, M. B.; Snaith, H. J. *Nature* **2013**, *501*, 395−398.
(26) Niu, G.; Li, W.; Meng, F.; Wang, L.; Dong, H.; Qiu, Y. *J. Mater. Chem. A* **2014**, *2*, 705−710.
(27) Noh, J. H.; Im, S. H.; Heo, J. H.; Mandal, T. N.; Seok, S. I. *Nano Lett.* **2013**, *13*, 1764−1769.
(28) Sun, S.; Salim, T.; Mathews, N.; Duchamp, M.; Boothroyd, C.; Xing, G.; Sum, T. C.; Lam, Y. M. *Energy Environ. Sci.* **2014**, *7*, 399−407.
(29) Bi, D.; Boschloo, G.; Schwarzmuller, S.; Yang, L.; Johansson, E. M. J.; Hagfeldt, A. *Nanoscale* **2013**, *5*, 11686−11691.
(30) Leijtens, T.; Eperon, G. E.; Pathak, S.; Abate, A.; Lee, M. M.; Snaith, H. J. *Nat. Commun.* **2013**, *4*, 2885.
(31) Janotti, A.; Van de Walle, C. G. *Phys. Rev. B* **2007**, *76*, 165202.
(32) Van de Walle, C. G.; Neugebauer, J. *J. Appl. Phys.* **2004**, *95*, 3851−3879.
(33) Stampfl, C.; Van de Walle, C. *Phys. Rev. B* **2002**, *65*, 155212.
(34) Farrell, D. E.; Wolverton, C. *Phys. Rev. B* **2012**, *85*, 174102.
(35) Dawson, J. A.; Harding, J. H.; Chen, H.; Sinclair, D. C. *J. Appl. Phys.* **2012**, *111*, 094108.
(36) Boukhvalov, D. W.; Solovyev, I. V. *Phys. Rev. B* **2010**, *82*, 245101.
(37) Na-Phattalung, S.; Smith, M.; Kim, K.; Du, M.-H.; Wei, S.-H.; Zhang, S.; Limpijumnong, S. *Phys. Rev. B* **2006**, *73*, 125205.
(38) Derenzo, S. E.; Bourret-Courchesne, E.; Yan, Z.; Bizarri, G.; Canning, A.; Zhang, G. *J. Lumin.* **2013**, *134*, 28−34.
(39) Kim, J.; Lee, S.-H.; Lee, J. H.; Hong, K.-H. *J. Phys. Chem. Lett.* **2014**, *5*, 1312−1317.
(40) Lany, S.; Zunger, A. *Phys. Rev. B* **2005**, *72*, 035215.
(41) Shockley, W.; Read, W. T. *Phys. Rev.* **1952**, *87*, 835−842.
(42) Zhitomirsky, D.; Voznyy, O.; Levina, L.; Hoogland, S.; Kemp, K. W.; Ip, A. H.; Thon, S. M.; Sargent, E. H. *Nat. Commun.* **2014**, *5*, 3803.
(43) Knop, O.; Wasylishen, R. E.; White, M. A.; Cameron, T.; Van Oort, M. J. *Can. J. Chem. 68*.
(44) Zhang, H.; Jang, J.; Liu, W.; Talapin, D. V. *ACS Nano* **2014**, *8*, 7359−7369.
(45) Zhitomirsky, D.; Voznyy, O.; Hoogland, S.; Sargent, E. H. *ACS Nano* **2013**, *7*, 5282−5290.
(46) Xing, G.; Mathews, N.; Sun, S.; Lim, S. S.; Lam, Y. M.; Grtzel, M.; Mhaisalkar, S.; Sum, T. C. *Science* **2013**, *342*, 344−347.
(47) Wehrenfennig, C.; Eperon, G. E.; Johnston, M. B.; Snaith, H. J.; Herz, L. M. *Adv. Mater.* **2013**, *26*, 1584−1589.
(48) Gonzalez-Pedro, V.; Juarez-Perez, E. J.; Arsyad, W.-S.; Barea, E. M.; Fabregat-Santiago, F.; Mora-Sero, I.; Bisquert, J. *Nano Lett.* **2014**, *14*, 888−893.
(49) Wojciechowski, K.; Saliba, M.; Leijtens, T.; Abate, A.; Snaith, H. *Energy Environ. Sci.* **2014**, *7*, 1142−1147.
(50) Loken, C.; et al. *J. Phys.: Conf. Ser.* **2010**, *256*, 012026.